CHEMISTRY
A EUROPEAN JOURNAL

DOI: 10.1002/chem.200802182

Single-Crystalline Molybdenum Trioxide Nanoribbons: Photocatalytic, Photoconductive, and Electrochemical Properties

Liang Cheng,[a] Mingwang Shao,*[a, b] Xiuhua Wang,[a] and Haibo Hu[a]

Abstract: Large-scale, high-purity and uniform α-MoO_3 nanoribbons have been synthesized by a facile hydrothermal route without employing surfactants or templates. The as-prepared α-MoO_3 nanoribbons were up to several micrometers in length, 100 nm in width, 15–20 nm in thickness, and grew along the [001] direction. The obtained nanoribbons exhibited a quantum size effect in optical properties, showing a blue shift of the band gap and direct transitions compared with the values of bulk MoO_3. The nanoribbons also showed superior photocatalytic ability in the photodegradation reaction of an aqueous solution of Rhodamine B under visible light. Furthermore, the as-prepared α-MoO_3 materials exhibited linear current–voltage (*I–V*) characteristics and excellent photoresponse. As the light source was switched on and off, the currents could be reversibly switched between high and low value at the voltage of 0.1 V. Electrochemical measurements predicted that the α-MoO_3/carbon fiber modified microelectrode would display excellent electrochemical characters and high sensitivity toward neurotransmitter dopamine. The modified electrode was also quite stable and had good reproducibility, which might have application in the electrochemical analysis.

Keywords: molybdenum oxides · nanostructures · photochemistry · photoresponse

Introduction

Over the past few decades considerable attention has been devoted to metal-oxide semiconductors, which have extremely important applications in various fields, such as field-effect transistors,[1] nanometersized ultrasensitive gas sensors,[2] resonators,[3] and high-efficiency catalysts.[4]

Among the various metal-oxide semiconductors, molybdenum trioxide (MoO_3) has attracted interest because of its multifaced functional properties. It has applications as a catalyst in selective oxidation reaction, secondary batteries, information display systems, sensors, lubricants, photochromic, and electrochromic systems.[5] Compared with the bulk counterpart, a significantly large surface area and high aspect ratio could be expected in 1D nanostructure. A variety of techniques have been developed to control the morphologies of MoO_3, for example the solvent thermal process, the electrochemical method, nanotubes templates, and acidification of ammonium heptamolybdate tetrahydrate.[6]

There are two basic polymorphisms of MoO_3. The fist one, orthorhombic MoO_3 (α-MoO_3), is a thermodynamically stable phase, and the second one, metastable monoclinic MoO_3 (β-MoO_3), has a ReO_3-type structure.[7] The most important structure characteristic of α-MoO_3 is its structural anisotropy, where highly asymmetrical MoO_6 octahedra are interconnected with their edges along [001] direction and interlinked with their corners along [100], resulting in a so-called double-layer planar structure. The feeble interactions between the double-layer sheets are mostly van der Waals forces.[6d]

In this paper, α-MoO_3 nanoribbons with the widths of 100 nm and the lengths of several micrometers were obtained through a simple hydrothermal route without any surfactant or template. The HCl solution plays an important role in the formation of α-MoO_3 nanoribbons. The optical properties of the product showed that as-prepared α-MoO_3 nanoribbons have good photo-catalytic activity for the degradation of Rhodamine B (RhB) under visible-light irradiation. The current–voltage (*I–V*) characteristics of α-MoO_3

[a] Dr. L. Cheng, Prof. M. Shao, X. Wang, H. Hu
Anhui Key Laboratory of Functional Molecular Solids
College of Chemistry and Materials Science
Anhui Normal University, Wuhu, 241000 (China)
Fax: (+86) 553-3869302
E-mail: mwshao@mail.ahnu.edu.cn

[b] Prof. M. Shao
Functional Nano and Soft Materials Laboratory (FUNSOM)
Soochow University, Suzhou 215123 (China)

Supporting information for this article is available on the WWW under http://dx.doi.org/10.1002/chem.200802182.

nanoribbons exhibited a good linear behavior and the photoswitching response was fast and reversible under on/off light exposure conditions. The electrochemical research of the products showed that α-MoO_3 nanoribbons could promote electron transfers between dopamine (DA) and the carbon fiber microelectrode. The modified electrode was quite stable and has good reproducibility, which might have application in the electrochemical analysis. This work could be of great importance for the exploration and expansion of potential applications of α-MoO_3.

Results and Discussion

The crystal structure and phase composition of the products were first characterized using X-ray powder diffraction (XRD). The XRD analysis of the as-prepared α-MoO_3 nanoribbons is shown in Figure 1a. All peaks can be indexed

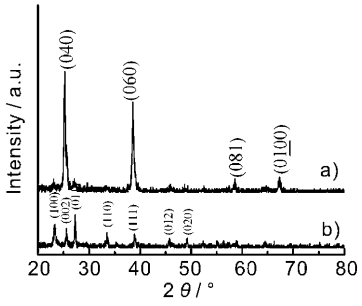

Figure 1. a) The XRD patterns of orthorhombic MoO_3 nanoribbons (JCPDS card, No. 05-0508), and b) monoclinic MoO_3 nanoribbons (JCPDS card No. 47-1320).

to orthorhombic structured MoO_3 (JCPDS card, No. 05-0508). No peaks of any other phase are detected, which indicated the purity of the final product. Compared with the standard XRD result, the stronger intensity of the reflection peaks of (02*k*0) indicates the anisotropic growth of the nanoribbons.

Field emitting scanning electron microscopy (FESEM) is employed to describe the morphologies of the products. The low magnification image of the as-synthesized α-MoO_3 nanoribbons, which displays a large quantity of ribbon-like MoO_3 nanostructures. The lengths are up to several micrometers. The yield of MoO_3 product was more than 95%. High magnification image (Figure 2b) shows that the product exhibits bending ribbon-like structures with uniform diameter of 100 nm and the thickness of 15–20 nm (Figure 2b, arrow). The surface of the nanoribbons is smooth. The chemical composition of these nanoribbons was checked by energy dispersive X-ray spectroscopy (EDS), as shown in Figure 2b. Besides the elements Si from substrate, only peaks of the elements Mo and O are detected in the EDS pattern.

A transmission electron microscopy (TEM) image of the prepared α-MoO_3 nanoribbons is shown in Figure 3, to

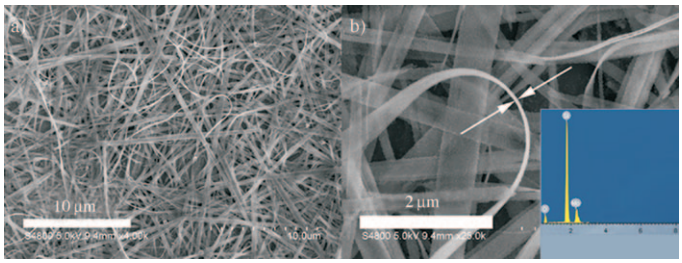

Figure 2. SEM images of α-MoO_3 with ribbon-like morphology: a) at low magnification, and b) at high magnification. Inset is the EDX spectrum of the α-MoO_3, indicating that the products are composed of Mo, and O elements. No peaks of other elements are detected in the spectrum, except Si from the silicon wafer, indicating the high purity of the product.

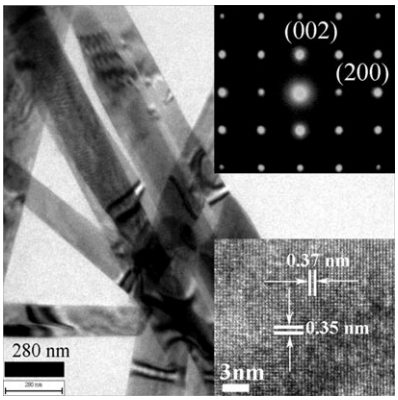

Figure 3. TEM image of the α-MoO_3 with the diameter 100 nm; HRTEM image of α-MoO_3 (lower inset) showing clear crystal lattice, which may be indexed as (111) and (2–20) crystal planes; and the SAED pattern (upper inset) suggesting single crystallinity of the α-MoO_3 nanoribbon.

reveal the ribbon-like morphology features. Each nanoribbon has a uniform width along its entire length, and the average width is ≈100 nm, which is confirmed by the SEM result. Selected area electron diffraction (SAED) (Figure 3, upper inset) recorded perpendicular to the growth axis can be indexed to the [010] zone of α-MoO_3, implying preferential growth along the *c*-axis. The SAED pattern further validates that the observed α-MoO_3 nanoribbons are single crystalline. The high-resolution TEM (Figure 3, lower inset) shows that the nanoribbons has lattice planes with spacings of 0.37 nm and 0.35 nm, corresponding to the *d* spacings of the (100) and (001) planes of the orthorhombic phase MoO_3 respectively. Further studies of the SAED and HRTEM image demonstrate that the nanoribbons grow along the [001] direction, which is consistent with the XRD results.

FTIR is also performed to investigate chemical bonding states between molybdenum and oxygen atoms in MoO_3 nanoribbons. The IR spectra of the as-synthesized MoO_3 nanoribbons is depicted in Figure 4. The signal at $\tilde{\nu}$ = 996 cm^{-1} is associated with the Mo=O stretching vibration, which is an indicator for the layered orthorhombic MoO_3 phase. The peak at $\tilde{\nu}$ = 868 cm^{-1} is assigned to the stretching

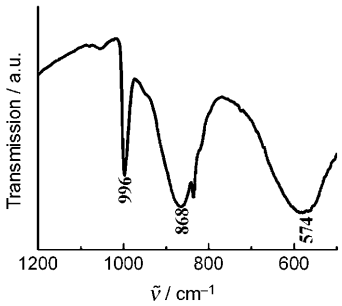

Figure 4. FTIR spectrum of the α-MoO_3 nanoribbons.

vibrations of the O atoms in the Mo-O-Mo units. The band at $\tilde{\nu}=574\ cm^{-1}$ is a result of the stretching vibrations of the O atoms linked to three metal atoms.[8] The Mo–O stretching vibration of interest could be explained as following; firstly, the mass of molybdenum atom is approximately six times that of an oxygen atom, so the vibration of the whole system is mainly attributed to the vibration of oxygen atoms. Secondly, the bond lengths of Mo–O in MoO_6 octahedra varies from 0.167 to 0.233 nm,[9] so the vibrations of oxygen atoms differ distinctly at un-equivalent positions. Therefore, the FTIR spectrum confirmed the formation of α-MoO_3.

To substantially understand the effect of pH on the growth of α-MoO_3 nanoribbons, contrasting experiments were carried out. At pH 7, only nanoparticles with large size were produced (Figure 5a), and the morphology of the products was still preserved even after the aging time was prolonged. As the usage of HCl was reduced (pH 5), the sample was essentially composed of α-MoO_3 nanoribbons with the diameters of ≈200–300 nm (Figure 5b), which was wider than the above nanoribbons with the reaction condition of pH 2. From these experimental results, it was observed that the presence of an appropriate amount of HCl played a crucial role in the growth of α-MoO_3 nanoribbons.

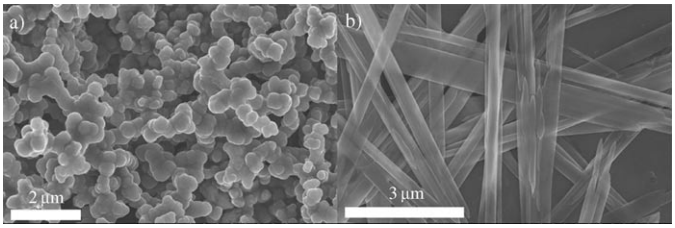

Figure 5. SEM images of α-MoO_3 samples with different pH value. a) pH 7 and b) pH 5.

To understand the growth mechanism of the nanoribbons accurately, it is necessary to investigate the morphology evolution of the intermediates involved in the formation. Figure 6a–c show the SEM images of the products obtained after reaction for 2, 5, and 8 h. After reaction for 2 h, the product was nanoparticles with diameters of 50–100 nm

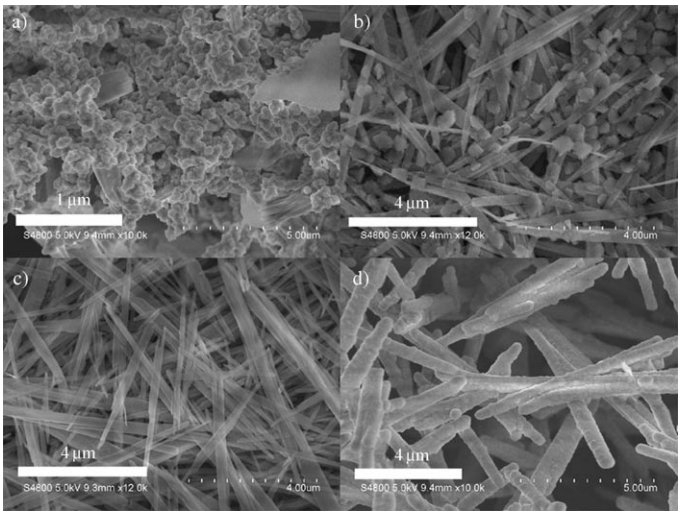

Figure 6. SEM images of three samples prepared after hydrothermal reaction for a) 2 h, b) 5 h, and c) 8 h, showing the morphological evolution of the MoO_3 nanoribbons. d) The SEM image of products obtained at the higher temperature 180 °C.

(Figure 6a). The XRD pattern (Figure 1b) can be assigned to metastable monoclinic (β-MoO_3, JCPDS card No. 47-1320). With an extension of the reaction time to 5 h, linear nanostructures were formed. As shown in Figure 6b, a great number of nanoparticles were attached on the circumference of linear structures, which suggested that the formation and growth of the linear nanostructures depended on the attached amorphous particles. If the reaction time was prolonged to 8 h, the nanoribbons became longer along their longitudinal axis, and their surfaces became smoother by continuously consuming the attached nanoparticles (Figure 6c). Eventually, the product evolved into pure nanoribbons with uniform diameters and length up to hundreds of micrometers (Figure 2). The reaction temperature is also a key factor in controlling the morphology of MoO_3 nanocrystals. Figure 6d shows the SEM image of the MoO_3 obtained at the higher temperature (180 °C) with other reaction conditions unchanged, the morphology of the final products were rod-like α-MoO_3 product with large size, and no nanoribbon could be observed.

Based on the time-dependent experiments, we proposed the formation mechanism. In the beginning, the reaction directly produces β-MoO_3 nanoparticles. Under the present hydrothermal conditions, β-MoO_3 nanoparticles partially dissolve in the solution and generate free MoO_3 molecules. If the concentration of MoO_3 molecules is high enough, MoO_3 molecules recrystallize and form crystalline MoO_3 molecule nuclei. The continuous feeding of MoO_3 molecules onto the crystalline seeds leads to the formation of linear nanostructures, resulting in the anisotropic crystal structure.[10] Additionally, the dissolution and sequential recrystallization process results in a transformation from β-MoO_3 to α-MoO_3. Such a growth process should be consistent with a solid–solution–solid transformation mechanism.[11]

From the above results, the favored [001] growth of α-MoO_3 is decided by its highly anisotropical structure. The orthorhombic structured α-MoO_3, with the space group *Pbnm* (D_{2h}^{16}),[12] has a distinct layered structure, which is seldom found in metal oxides. In α-MoO_3, distorted MoO_6 octahedrons share both edges (along [001] direction) and corners (along [100] direction). The interactions between layers along *b*-axis are weak van der waals forces. From the energy viewpoint, the corresponding energy release along [001] is much greater than the [100] direction.[13] Planar growth rates along axes of the crystal have the following sequence {001}> {100} > {010},[14] so the nanoribbons grow along [001] direction are much favored. The XRD diffraction of ($0k0$) planes is much stronger than that of other planes, since the (010) plane is retained in the final product as the consequence of slow growing rate. The 1D growth may be induced by the absorption of H^+ cation to the (010) plane, which will accelerate the growth by changing the degree of supersaturation round the side surfaces.

The UV/Vis diffuse reflectance spectrum of the as-prepared monoclinic MoO_3 nanoribbons is displayed in Figure 7a. As a crystalline semiconductor, the optical absorption near the band edge follows the formula $\alpha h\nu = A(h\nu - E_g)^{n/2}$,[15] in which α, ν, E_g and A are the absorption coefficient, light frequency, band gap and a constant, respectively. Among them, the value of n depends on the characteristics of the transition in a semiconductor, that is, direct transition ($n=1$) or indirect transition ($n=4$). For α-MoO_3, the value of n is one.[16] From the curve of the $(\alpha h\nu)^2$ versus photon energy ($h\nu$) of α-MoO_3 nanoribbons (Figure 7b), $(\alpha h\nu)^2$ versus ($h\nu$) for α-MoO_3 nanoribbons can yield straight-line plot, and the band gap E_g of α-MoO_3 can be thus estimated from a plot $(\alpha h\nu)^2$ versus ($h\nu$). The intercept of the tangent to the *x*-axis will give a good approximation of the band gap E_g, so the estimated band gap E_g of α-MoO_3 nanoribbons is 3.18 eV, which is large than the value for the bulk material.[9a] The blue shift of the band gap and direct transitions indicate quantum confinement effects in the nanostructure obtained.

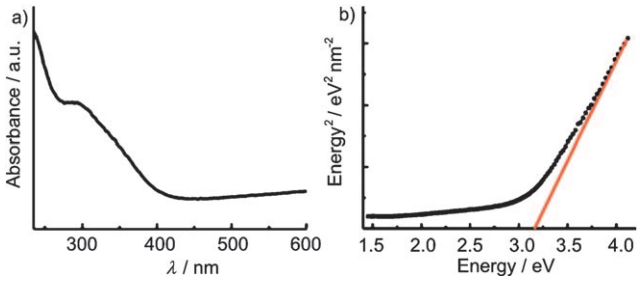

Figure 7. a) UV/Vis spectrum of as-prepared α-MoO_3 nanoribbons mixed with $BaSO_4$ powder at room temperature. b) Plots of the $(\alpha h\nu)^2$ versus photon energy ($h\nu$) for as-prepared α-MoO_3 nanoribbons.

Photocatalytic properties of the as-prepared samples were examined by degradation of RhB dye solution under visible-light irradiation at room temperature. The characteristic absorption of RhB at $\lambda = 552$ nm was chosen to monitor the photocatalytic degradation process. The absorption spectra of an aqueous solution of RhB exposed to visible-light irradiation for various time periods is shown in Figure 8. The

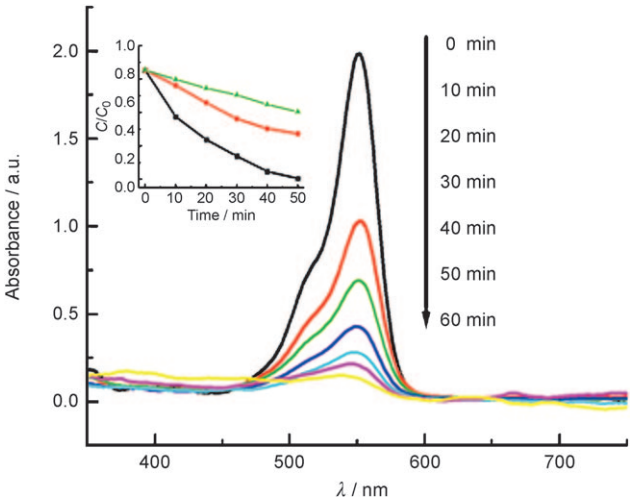

Figure 8. Absorption spectra of the RhB solution under UV visible light irradiation in the presence of as-prepared α-MoO_3 nanoribbons. Inset: Comparison of the change in RB concentration under different catalytic Conditions: ▲=P25, ●=bulk MoO_3 particles, and ■=α-MoO_3 nanoribbons.

absorption peak at $\lambda = 552$ nm diminished gradually as the visible-light irradiation time increases, and completely disappeared after about 1 hour. No new absorption bands appeared in either the visible or ultraviolet regions, which indicated the complete photocatalytic degradation of RhB during the reaction.

We also used commercial TiO_2 (commercial Degussa P25 TiO_2) and bulk MoO_3 particles as references to evaluate the photocatalytic performance of α-MoO_3 nanoribbons. As illustrated in the inset of Figure 8, it is clear that α-MoO_3 nanoribbons exhibit superior photocatalytic abilities over P25 and bulk MoO_3. This implies that the as-prepared α-MoO_3 nanoribbons have a large surface area.

Nanoribbons, which have large surface areas and, therefore, an extremely high absorption capacity, are useful for the collection of organic pollute molecules like RhB. Under visible light irradiation, the electrons were transferred from the valence band to the conduction band of the α-MoO_3 nanoparticles connected to these nanoribbons. The injected energy was captured by the surface adsorbed molecular O_2, to yield $O_2^{\bullet-}$ and $HOO^{\bullet-}$ radical ions. Then the RhB molecules could be mineralized timely by the radical ions. Because of the high absorption capacity and increase in the amount of excited electrons in α-MoO_3 nanoribbons, the RhB molecules absorbed on the surface of α-MoO_3 will be easily photodegraded.

To measure the current signals through the α-MoO_3 nanoribbons, an indium tin oxide (ITO) coated glass with the electrode gap of 25 μm was employed as the substrate. A

bundle of α-MoO_3 nanoribbons was dispersed and bridged over the electrodes with effective length of 60 μm as shown in Figure 9a (inset). To increase injection of the device, Au

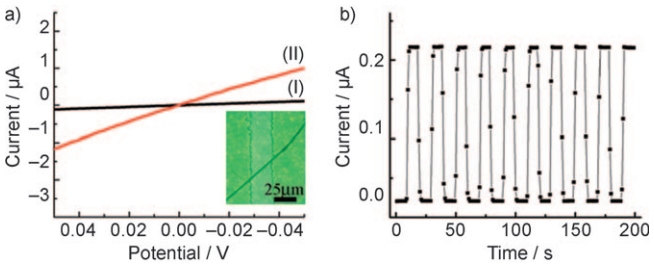

Figure 9. a) *I–V* curves of a bundle of α-MoO_3 nanoribbons measured in the dark (curve I, ——) and under illumination by using an incandescence lamp (12 V, 10 W) (curve II, ——), and the image of a bundle of α-MoO_3 nanoribbons bridging over ITO electrodes from an optical microscope (inset). b) Photoconductive characteristics of the device during light switching on/off. A voltage of 0.1 V was applied across the Au-Au electrodes and the current was recorded during the light alternatively on and off at 10 s intervals.

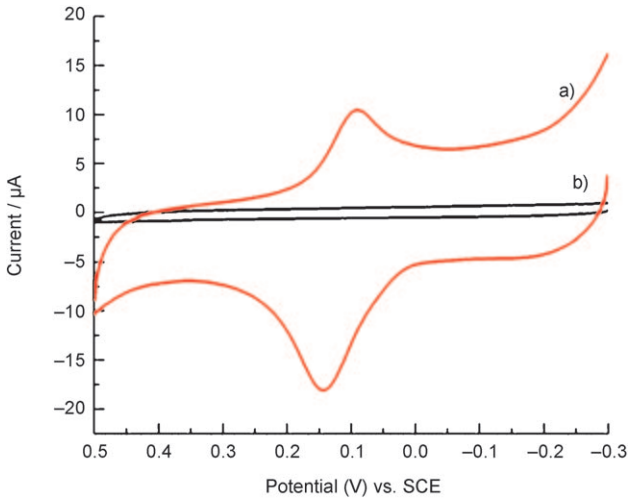

Figure 10. Cyclic voltammograms for 10^{-5} M DA in PBS (pH 7.4) at a) α-MoO_3 modified CFME (——), b) bare CFME (——), and the scan rate is 0.05 V S^{-1}.

gap electrodes were fabricated on the substrate by thermal evaporation with a micrometer-sized Au wire as the mask; by slightly moving the Au-wire mask, Au–Au gap electrodes were deposited. To decrease the thermal effect, the distance between the nanoribbons and the light source was 10 cm and the power of the incandescence lamp was only 10 W. Figure 9a shows the *I–V* curves measured in the dark (curve I) and under illumination (curve II) for comparison. Both of them exhibit good linear behavior, which establishes that there is a fine ohmic contact between the α-MoO_3 nanoribbons and Au electrodes. The conductivity of the nanoribbons rapidly increased under illumination with an incandescence lamp. In these cases, the energy from the light excites the electrons in the semiconductor α-MoO_3 nanoribbons from the valence band into the conduction band, increasing the charge-carrier concentration through direct electron–hole pair creation and thus enhancing the conductivity of the nanoribbons.

The reversible photoconductive characteristics of the α-MoO_3 nanoribbons is shown in Figure 9b. A voltage of 0.1 V was applied across the two electrodes and the current recorded during the light was alternatively on and off at 10 s intervals. Obviously, the current through the α-MoO_3 nanoribbons promptly increased and decreased according to the illumination on and off, which proves that the device is highly sensitive and its behavior is repeatable. The measurements were performed for ten periods and showed that the photoconduction behavior was reproducible. The photoconductivity characteristics suggest that the α-MoO_3 nanoribbons are good candidates for optoelectronic switches.

Cyclic voltammetry (CV) was performed to characterize the electrochemical behavior of α-MoO_3 nanoribbons as shown in Figure 10. The carbon fiber microelectrode (CFME) was constructed as previously described (Figure S1 in the Supporting Information), and the electrode modified with α-MoO_3 nanoribbons was also prepared (Figure S2 in the Supporting Information). A pair of distinct redox peaks could be found if the bare CFME electrode was used as the working electrode (curve a). Although α-MoO_3 nanoribbon-modified CFME was used as the working electrode, the peak currents obviously enhanced, and the anodic and cathodic peak potentials are 143.89 mV and 89.51 mV, respectively, which has a negative direction shift for the anodic peak potential and positive shift for cathodic, in comparison with the bare CFME (curve b); the difference (ΔEp) between Epa and Epc is 54.38 mV. In addition, the peak currents enhance remarkably. The above experiments indicated that the as-prepared α-MoO_3 nanoribbons could promote the electron transfer between DA and CFME, namely the product has good electrochemical properties.

To test the response of α-MoO_3/CFME for DA more accurately, differential pulse voltammetry (DPV) experiments were carried out. DPV recordings at various DA concentrations at the α-MoO_3/CFME electrode in PBS (pH 7.4) are shown in Figure 11. A series of well-defined peaks are obtained, owing to the good reversibility of the α-MoO_3 nanoribbon-modified CFME. The response of DA was linear in the range between 8.0×10^{-6} to 7.2×10^{-5} M, and the linear regression equation is i_{pa} (μA) $= 6.36 + 0.064\,C_{DA}$ (μM), with a correlation coefficient of 0.9954. The detection limit of DA was 1.0×10^{-7} M. This should be attributed to the large available surface area of the modified electrode and the excellent electrical properties of the α-MoO_3 nanoribbons.

Conclusion

In summary, high purity and uniform α-MoO_3 nanoribbons with the diameters of ≈100 nm and lengths up to several micrometers were successfully synthesized under the hydrothermal conditions without any template and surfactant. The

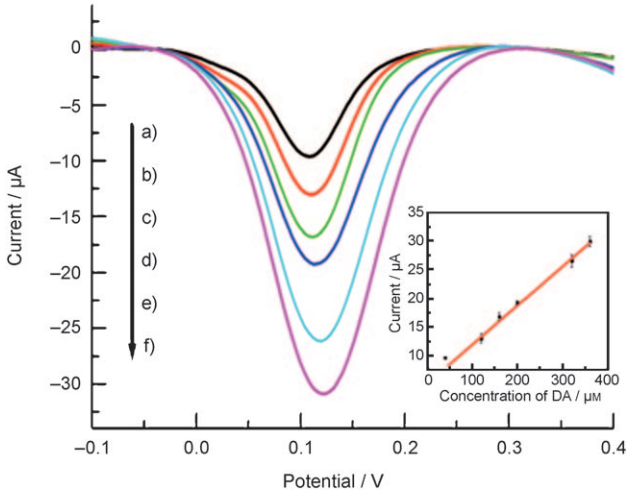

Figure 11. DPV with α-MoO_3/CFME in a pH 7.4 PBS at different concentrations of DA: a) 8; b) 24; c) 32; d) 40; e) 64; and f) 72 μM, and the linear plot of peak current versus concentration of DA (inset).

pH and reaction time might play a key role in the process of crystal growth. The growth mechanism could be ascribed to a solid–solution–solid transformation mechanism. Furthermore, the as-prepared nanoribbons exhibited superior photocatalytic activity for the degradation of RhB under visible light irradiation, which may be attributed to the distinctive morphology that results in a large surface area. The photoswitchable conductivity of a bundle of α-MoO_3 nanoribbons exhibited a unique photoswitching response, which was both fast and reversible under on/off light exposure conditions. The α-MoO_3/CFME modified electrode displayed excellent electrochemical character and showed very high sensitivity toward neurotransmitter DA. The modified electrode was quite stable and had good reproducibility. This method offers a simple, economical, and convenient way to obtain high-quality detectors for bioelectroanalysis, capillary electrophoresis, miniaturized total analysis systems, and other fields.

Experimental Section

All the reagents in the experiments were analytically pure, purchased from Shanghai Chemical Company, and used without further purification. A typical synthetic procedure was as follows: Na_2MoO_4 (0.1 g) was dissolved in distilled water (30 mL) under stirring for 0.5 h, then HCl (10 mL, 0.2 M) was added under magnetic stirring. The resultant solution was transferred into a stainless steel autoclave (50 mL capacity), kept at 160 °C for 20 h, and then cooled to room temperature naturally. The resultant precipitate was collected, washed with distilled water, absolute ethanol, and acetone thoroughly and finally dried under vacuum at 60 °C for 10 h. For comparison, reactions with various times and temperature had been conducted, while other conditions kept unchanged.

The phase and crystallography of the products were characterized by using a Shimadzu XRD-6000 X-ray diffractometer equipped with $Cu_{K\alpha}$ radiation ($\lambda = 0.15406$ nm). A scanning rate of 0.05° s^{-1} was applied to record the pattern in the 2θ range of 20–80°. The scanning electron microscopy (SEM) images were taken by using an S-4800 field emitting scanning electron microscope equipped with an energy dispersive X-ray (EDX) spectrum. Transmission electron microscopy (TEM), selected area electron diffraction (SAED) pattern and high-resolution transmission electron microscope (HRTEM) image were captured by using a JEOL-2010 transmission electron microscope, using an accelerating voltage of 200 kV. The low magnification image was taken from an Olympus optical microscope. Fourier transform infrared (FTIR) absorption spectrum of the nanoribbons was recorded by using a 60-SXB IR spectrometer of 4 cm^{-1} resolution, over a wave number range of 500–1200 cm^{-1}.

UV/Vis diffuse reflectance spectrum was measured on a Hitachi U-2050 spectrophotometer at room temperature. A small amount of α-MoO_3 nanoribbons were dispersed in $BaSO_4$ for UV/Vis absorbance spectroscopy measurement in the wavelength range between 200 and 600 nm.

To investigate the photocatalytic activity of the samples, an investigation of RhB, in the presence of α-MoO_3 nanoribbons, under visible-light irradiation was carried out at room temperature. A 250 W GaI_3 lamp (DJG250, Shanghai Hualun Lighting Company, China) with maximum radiant wavelength matches to the absorption wavelength of PFT was put into a cylindrical glass vessel as the visible light source with a recycling glass water jacket to avoid overheating. A UV and IR cut-off filter was placed between the lamp and the reaction solution to ensure irradiation by visible light (400–700 nm) only. The photocatalytic experiment was carried out by adding photocatalyst (50 mg) to an aqueous RhB solution (50 mL, 10 mg L^{-1}) with an initial concentration of. Prior to illumination, the suspension was magnetically stirred for an hour in dark to establish an absorption/desorption equilibrium of RhB. Subsequently, the dispersion containing RhB and photocatalyst was irradiated under visible light. At given intervals, 3 mL of the suspensions were extracted and subsequently centrifuged at a rate of 9000 rpm for 15 min. UV/Vis absorption spectra of the supernatant were then measured using a Shimadzu U-4100 UV/Vis absorbance spectroscopy.

The photoconductivity measurements were tracked with a CHI 620B (CHI Instruments, Chenhua Corporation, Shanghai, China) electrochemical workstation. A bundle of MoO_3 nanoribbons was dispersed and bridged over the ITO electrodes. Light was supplied with incandescence lamp (12 V, 10 W).

The electrochemical measurement was performed by using a CHI 620B Electrochemical Workstation with three-electrode system consisting of a Ag/AgCl as a reference electrode, a platinum wire as a counter electrode and a bare or modified CFME as a work electrode employing a scanning rate of 100 mV s^{-1} and the rest time of 2 s. Prior to the experiment, solutions were purged with nitrogen for 30 min to remove oxygen.

Acknowledgements

The project was supported by the National Natural Foundation of China (20571001), the National Basic Research Program of China (973 Program) (Grant No. 2006CB933000), and Anhui Provincial Natural Science Foundation (070414185).

[1] a) Z. W. Pan, Z. R. Dai, Z. L. Wang, *Science* **2001**, *291*, 1947–1949; b) J. S. Jie, W. J. Zhang, Y. Jiang, X. M. Meng, Y. Q. Li, S. T. Lee, *Nano Lett.* **2006**, *6*, 1887–1892.

[2] a) E. S. Snow, F. K. Perkins, E. J. Houser, S. C. Badescu, T. L. Reinecke, *Science* **2005**, *307*, 1942–1945; b) Y. Zhao, Y. Xie, X. Zhu, S. Yan, S. X. Wang, *Chem. Eur. J.* **2008**, *14*, 1601–1606; c) X. L. Gou, G. X. Wang, X. Y. Kong, D. Wexler, J. Horvat, J. Yang, J. Park, *Chem. Eur. J.* **2008**, *14*, 5996–6002; d) D. J. Sirbuly, A. Tao, M. Law, R. Fan, P. D. Yang, *Adv. Mater.* **2007**, *19*, 61–66; e) Q. Kuang, C. S. Lao, Z. L. Wang, Z. X. Xie, L. S. Zheng, *J. Am. Chem. Soc.* **2007**, *129*, 6070–6071.

[3] X. D. Bai, P. X. Gao, Z. L. Wang, E. G. Wang, *Appl. Phys. Lett.* **2003**, *82*, 4806–4808.

[4] a) H. Yan, J. Johnson, M. Law, R. He, K. Knutsen, J. R. McKinney, J. Pham, R. Saykally, P. D. Yang, *Adv. Mater.* **2003**, *15*, 1907–1911; b) Z. Y. Liu, D. D. Sun, P. Guo, J. O. Leckie, *Chem. Eur. J.* **2007**, *13*, 1851–1855.
[5] a) H. F. Liu, R. S. Liu, K. Y. Liew, R. E. Johnson, J. H. Lunsford, *J. Am. Chem. Soc.* **1984**, *106*, 4117–4121; b) T. A. Kerr, F. Leroux, L. F. Nazar, *Chem. Mater.* **1998**, *10*, 2588–2591; c) X. W. Lou, H. C. Zeng, *J. Am. Chem. Soc.* **2003**, *125*, 2697–2704; d) K. Hosono, I. Matsubara, N. Murayama, S. Woosuck, N. Izu, *Chem. Mater.* **2005**, *17*, 349–354; e) J. Wang, K. C. Rose, C. M. Lieber, *J. Phys. Chem. A* **1999**, *103*, 8405–8409; f) J. N. Yao, Y. A. Yang, B. H. Loo, *J. Phys. Chem. A* **1998**, *102*, 1856–1860; g) Y. A. Yang, Y. W. Cao, B. H. Loo, J. N. Yao, *J. Phys. Chem. A* **1998**, *102*, 9392–9396.
[6] a) A. Michailovski, J. D. Grunwaldt, A. Baiker, R. Kiebach, W. Bensch, G. R. Patzke, *Angew. Chem.* **2005**, *117*, 5787–5792; *Angew. Chem.* **2005**, *44*, 5643–5647; b) T. M. McEvoy, K. J. Stevenson, *J. Mater. Res.* **2004**, *19*, 429–438; c) B. C. Satishkumar, A. Govindaraj, M. Nath, C. N. R. Rao, *J. Mater. Chem.* **2000**, *10*, 2115–2119; d) J. Zhou, N. S. Xu, S. Z. Deng, J. Chen, J. C. She, Z. L. Wang, *Adv. Mater.* **2003**, *15*, 1835–1840.
[7] X. W. Lou, H. C. Zeng, *Chem. Mater.* **2002**, *14*, 4781–4789.
[8] K. Eda, *J. Solid State Chem.* **1991**, *95*, 64–73.
[9] a) L. Seguin, M. Figlarz, R. Cavagnat, J.-C. Lasse′gues, *Spectrochim. Acta* **1995**, *51*, 1323; b) L. Q. Mai, B. Hu, W. Chen, Y. Y. Qi, C. S. Lao, R. S. Yang, Y. Dai, Z. L. Wang, *Adv. Mater.* **2007**, *19*, 3712–3716.
[10] B. Gates, B. Mayers, B. Cattle, Y. N. Xia, *Adv. Funct. Mater.* **2002**, *12*, 219–227.
[11] Q. Xie, Z. Dai, W. W. Huang, W. Zhang, D. K. Ma, X. K. Hu, Y. T. Qian, *Cryst. Growth Des.* **2006**, *6*, 1514–1517.
[12] Q. P. Ding, H. B. Huang, J. H. Duan, J. F. Gong, S. G. Yang, X. Z. Zhao, Y. W. Du, *J. Cryst. Growth* **2006**, *294*, 304–308.
[13] X. L. Li, J. F. Liu, Y. D. Li, *Appl. Phys. Lett.* **2002**, *81*, 4832–4834.
[14] H. C. Zeng, *J. Cryst. Growth* **1998**, *186*, 393–402.
[15] M. A. Butler, *J. Appl. Phys.* **1977**, *48*, 1914–1920.
[16] L. Zhou, W. Z. Wang, S. W. Liu, L. S. Zhang, H. L. Xu, W. Zhu, *J. Mol. Catal. A* **2006**, *252*, 120–124.

Received: October 21, 2008
Published online: January 20, 2009

